Sodium Voiding Analysis in KALIMER

Chang, Won-Pyo, Jeong, Kwan-Seong, Hahn, Dohee

Korea Atomic Energy Research Institute
P.O.Box 105, Yusung, Taejon, 305-600, Korea
wpchang@kaeri.re.kr

Key words : Sodium Boiling, KALIMER, SSC-K, HCDA, Reactivity Feedback

A sodium boiling model has been developed for calculations of the void reactivity feedback as well as the fuel and cladding temperatures in the KALIMER core after onset of sodium boiling. The sodium boiling in liquid metal reactors using sodium as coolant should be modeled because of phenomenon difference observed from that in light water reactor systems. The developed model is a multiple-bubble slug ejection model. It allows a finite number of bubbles in a channel at any time. Voiding is assumed to result from formation of bubbles that fill the whole cross section of the coolant channel except for liquid film left on the cladding surface. The vapor pressure, currently, is assumed to be uniform within a bubble. The present study is focused on not only demonstration of the sodium voiding behavior predicted by the developed model, but also confirmation on qualitative acceptance for the model. In results, the model catches important phenomena for sodium boiling, while further effort should be made for the complete analysis.

1. Introduction

The Korea Atomic Energy Research Institute (KAERI) has been developing a conceptual design of KALIMER (**K**orea **A**dvanced **LI**quid **ME**tal **R**eactor) [1], which is a sodium cooled, 150 MWe, pool-type reactor. The primary heat transport system (PHTS) of KALIMER is submerged in the big sodium pool, which provides the large thermal inertia of the system. KALIMER, with a metallic fueled core, is designed in such a way that intrinsic negative reactivity feedback effect is expected during the transients including design basis events.

Even though the KALIMER design may not allow boiling at any circumstance under the design basis accidents, sodium boiling is anticipated under HCDA (Hypothetical Core Disruptive Accident) initiating events which are represented by UTOP(Unprotected Transient Over Power), ULOF(Unprotected Loss Of Flow),

ULOHS(Unprotected Loss Of Heat Sink), or sudden flow channel blockage, due to power excursion caused by the reactivity feedback. For realistic assessment of the HCDA consequence, it is important to predict the core void in order to estimate the core reactivity feedback.[2] The slug and annular flow regimes tend to prevail for liquid-metal boiling near atmospheric pressure, while the bubbly flow is typical under high pressure in light water reactors.[3,4] In this regard, sodium voiding in liquid metal reactors should be modeled because of phenomenon difference observed from that in light water reactor systems. Unfortunately, SSC-K [5] which is used as the main code for KALIMER safety analysis is not capable of analyzing the sodium boiling in the core so far. To this end, the sodium boiling model has been developed in order to extend the applicable range of SSC-K.

There are a few codes capable of analyzing the HCDA initiating events. SAS series [6] and FRAX [7,8,9] codes may be representatives on this area. They basically use the multi-bubble slug ejection model, which represents the boiling coolant with multi liquid slugs divided by bubbles.

2. Development of Sodium Boiling Model (SOBOIL)

The Sodium boiling model in SOBOIL is basically the multi-bubble slug ejection model similar to that used in SAS2A.[4] The model adopts a more general approach for calculation of conduction heat transfer in a fuel pin or structure. Because the interfaces between the liquid slug and vapor bubble are moving, modeling which uses only fixed nodes are not likely to be good enough. Fig. 1 represents the nodalization for the numerical method used in SOBOIL. Voiding is assumed to result in formation of bubbles that fill the whole cross section of the coolant channel except for a film left on the cladding or on the structure. Finite numbers of bubbles, separated by liquid slugs, are allowed in the channel at any time. The liquid film around the vapor is assumed to be static currently, its motion, however, will be improved later.

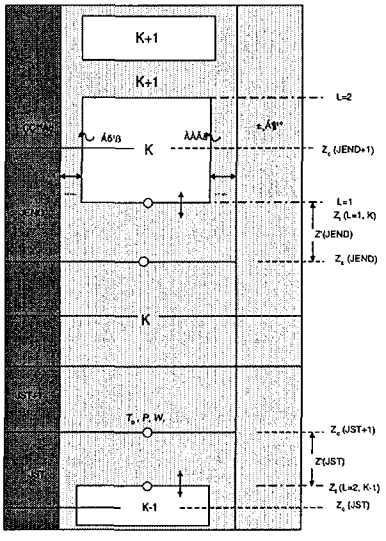

Fig. 1 Nodalization for SOBOIL Model

(1) Liquid Slug Flow Rates

The description of the momentum conservation equation for the liquid flow is similar to that used in SAS2A [4], except expressing it with the flow rate instead of mass flux in order to take account of the flow area variation for a node in the

numerical computation. The liquid momentum equation is given by

$$\frac{1}{A_c}\frac{W}{t}+\frac{P}{z}+\frac{1}{A_c}\frac{(Wv)}{z}= \quad \frac{P}{z}\div_{fr} \quad \frac{P}{z}\div_{K} \quad p_c g \tag{1}$$

The integral momentum equation is applied to each slug (slug K) shown in Fig. 1, and is integrated over the length of each slug, individually. Thus, a flow rate exists in a liquid slug. The integer variable JST is the number of the mesh segment at which the bottom of the liquid slug is located, while JEND is the number of the segment in which the upper interface is contained. In Eq. (1), the change in the flow rate for a liquid slug is related to changes in vapor pressures above and below the liquid slug. Once the flow change, w, is known from the numerically approximated equation for Eq. (1), the coolant pressures at all the nodes can be subsequently determined.

(2) Liquid Temperature

Since the interface moves along the axis, both Eulerian and Lagrangian schemes are used for computing transient temperatures in the liquid slugs. The Eulerian scheme is usually applied before incipient boiling, while the Lagrangian scheme is used for all liquid slugs other than the inlet liquid slug after boiling. However, Lagrangian scheme is also used for the inlet liquid slug when the flow rate is small (~ 10 % of the initial flow rate).

For the Eulerian scheme, the basic energy equation in a liquid slug is given by

$$\mathrm{r}_{\ell} c_{\ell}\frac{T_c}{t} + Gc_{\ell}\frac{T_c}{z} = \mathrm{j}\,(z,t) + Q_c(z,t) \tag{2}$$

Eq. (2) is numerically discritized with semi-implicit method in time and space to find the coolant temperatures at the fixed mesh points.

The Lagrangian scheme is used to calculate the liquid coolant temperatures both at the fixed axial mesh points and at moving points near the liquid-vapor interfaces. Total time derivative for the Lagrangian scheme, dT_c/dt, as seen by an observer moving with the coolant velocity, is used to solve the interface liquid temperature, $T_{ci}(t+\ t)$. Axial heat conduction through the interfaces is ignored in the calculation of the interface liquid temperatures. This derivative is accordingly approximated by;

$$\frac{dT_c}{dt} = \frac{T_c(z,t+\ t)\quad T_c(z\quad z,t)}{t} \tag{3}$$

where

$$z = \frac{[G(t+\ t)+G(t)]\ \ t}{2\,\mathrm{r}\,(z)}, \qquad \mathrm{r}\,(z)=\mathrm{r}\,(T_c(z,t+\ t/2)) \tag{4}$$

The basic equation for the interface liquid temperature, $T_{ci}(t+\ t)$, by the Lagrangian formulation is numerically approximated by

$$\mathrm{r}\ c\frac{T_{ci}(t+\ t)\ \ T_{ci}(t)}{t} = \frac{1}{2}[\mathrm{j}\ (t+\ t)+\mathrm{j}\ (t)] + Q_c \tag{5}$$

where j are now defined as

$$\mathrm{j}\ (t+\ t) = h_{eci}(t+\ t)[T_{ei}(t+\ t)\ \ T_{ci}(t+\ t)] \tag{6}$$

$$\mathrm{j}\ (t) = h_{eci}(t)[T_{ei}(t)\ \ T_{ci}(t)] \tag{7}$$

The subscript i refers to values at the interfaces and T_{ei}, T_{ci}, and h_{eci} indicate wall temperature, coolant temperature, and heat transfer coefficient between wall and coolant, respectively. Since the cladding and structure temperatures are only calculated at the fixed axial mesh points, T_{ei} is obtained by linear interpolation from the mesh-point values. The values of $\bar{r}$ and $\bar{c}$ are obtained using the extrapolated interface temperature at $t+\ t/2$.

The Lagrangian calculation for the coolant temperatures at fixed axial mesh points is similar to Eq. (5) and the resulting equation is given by

$$T_c(z,t+\ t) = \frac{T_c(z\ \ z,t)(1\ \ d_1 h_1)+d_1\mathrm{j}_{\ 1}}{1+d_1 h_2} \tag{8}$$

where, z is given by Eq. (4), and the temperatures $T_c(z - z, t)$ and $T_e(z - z, t)$ are obtained by linear interpolation from the values at the fixed mesh points. For heat conduction calculation, the one-dimensional heat conduction equation is set up in order to calculate temperature distribution within the fuel pin or structure with given boundary conditions in a cylindrical coordinate. Successive iteration method is used for the numerical method in solving the equation. The maximum 50 nodes in the radial direction are currently allowed.

(4) Basic Assumptions for Vapor Bubble Modeling

The present SOBOIL model is developed based on a model which assumes the pressure is uniform spatially inside a vapor, and so is adequate to small bubbles. A vapor is modeled to be formed if the local coolant temperature exceeds a specified amount of superheat at the node. Then, calculations of the coolant temperature are repeated for the time step, so as to satisfy the superheat criterion exactly at the end of time step. This model, however, is developed under the following assumptions.

(i) No new vapor will be formed within a minimum distance adjacent to a vapor-liquid interface, and, thus, nodes within the distance from the interfaces are not examined for bubble formation ;

(ii) No more than one bubble will be formed within a time-step;

(iii) If the change of the liquid flow rate is larger than 30 %, the time step is reduced and repeat the calculation;

(vi) If a vapor temperature change exceeds a specified amount, the time-step is also reduced.

(v) A new vapor generated in a liquid slug divides the liquid slug into two liquid slugs and the initial liquid flow rates for these two liquid slugs are assumed same as that of the liquid slug before the voiding.

(vi) Vapors are always saturated at given temperatures.

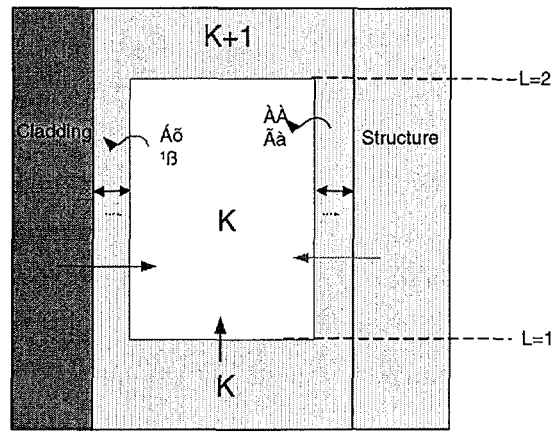

Fig. 2 Uniform Vapor Pressure Bubble Model

The shrink of a vapor bubble is possible because of condensation in the cooler region. When the vapor length and the decreasing rate of the vapor is simultaneously below a minimum value, the vapor disappears. Two liquid slugs are also combined into one if the gap distance between two vapors is close enough each other.

The bubble growth is determined by coupling the momentum equations for the liquid slugs with energy balances in the vapor bubbles, assuming saturation conditions, and spatially uniform pressure and temperature within a bubble. The rates of formation and condensation of vapor are determined by the heat flows through the liquid film on the cladding or structure and through the liquid-vapor interfaces. Fig. 2 shows the control volume considered in the uniform vapor pressure model. The control volume extends from the lower liquid-vapor interface to the upper one, and from one outer surface of the heat structure to the other one. The primary focus of

this model is to obtain the temperatures within vapor bubbles. Once the temperatures are known, they can be used to calculate the vapor pressure, since saturation conditions are assumed. The vapor pressure is the driving force for motion of the liquid slugs, and so finding the vapor pressures provides the link conditions between in the liquid slugs and conditions in the vapors. Therefore, they lead to a complete description of conditions throughout the channel.

(5) Energy transfer into the uniform pressure bubble

The total energy added to a vapor bubble K in a time step is

$$E_t = \int_{t}^{t+\Delta t} [\, Q_{es}(t) + Q_i(t) \,]\, dt \tag{9}$$

Q_{es} and Q_i are the heat flow from the heat structure and interface heat flow, respectively. Q_{es} is approximated by

$$Q_{es} = \frac{\Delta t}{2}\, Q_{es}(k,t) + Q_{es}(k,t+\Delta t) \tag{10}$$

$$Q_{es}(k,t) = P_e \int_{Z_i(L=1,t,K)}^{Z_i(L=2,t,K)} q_e(z,t)\, dz \tag{11}$$

with $z_i(2,t,K)$ = height of upper liquid-vapor interface,
$z_i(1,t,K)$ = height of lower liquid-vapor interface,
P_e = perimeter of cladding = 2 r_e,
r_e = nominal radius of cladding, and
q_e = cladding-to-vapor heat flux.

(6) Heat Flow through Liquid-vapor Interface

SOBOIL model for calculation of interfacial heat transfer between liquid and vapor is directly based on that in SAS2A [2]. In this method, the total heat flow through the liquid-vapor interfaces is the sum of an upper interface term I_{iu} and a lower interface term $I_{i\ell}$

$$Q_i = \Delta t (I_{iu} + I_{i\ell}) \tag{12}$$

where, $I_{ix} = k_\ell A_{cx} \left.\frac{\overline{T}_{\ell x}}{x}\right|_{x=0}$ (13)

The heat conduction equation near the interface may be written as;

$$a \frac{\partial^2 T_2(x, t)}{x^2} + \frac{Q(x, t)}{r_2 C_2} = \frac{T_\ell(x, t)}{t} \quad (14)$$

The heat equation, together with the initial and boundary conditions, can be solved for T_ℓ through the use of the Laplace transform method. An expression for the coolant temperature derivative $\frac{\overline{T}_{\ell x}}{x}$ can also be derived from Eq. (14).

(7) Change in Vapor Energy

The heat flow into the control volume of a vapor is used both to produce a new vapor and to raise the temperature of already existing vapor. During a time interval t, the vapor temperature goes from T to T+ T, the pressure goes from P_V+ P, the density goes from $_V$+ $_V$, the vapor volume goes from V_v to V_v+ V, and the vapor energy changes by E. The changes of ¡ ÊP and ¡ â$_v$ are related to ¡ ãT by the requirement that saturation conditions prevail in the vapor.

Two processes contribute to the energy change ¡ ÊE. One is the heating of the quantity of vapor present at the beginning of the time step from temperature T to temperature T+¡ ãT. The other is the vaporizing of some of the liquid film to from additional vapor, giving a total vapor mass of ($_v$+ ¡ â$_v$) (V_v+¡ ÊV) at the end of the time step.

(8) Energy Balance

The energy balance between the energy transferred to the control volume and the energy change within the volume, determines the change of the vapor energy. The energy transferred to the volume, E_t, is the sum of energy flow from the cladding or structure, Q_{es}, and the energy flow through the liquid-vapor interfaces, Q_i, in Eq. (9). The E_t further can be expressed as a linear function of the change in the vapor temperature, T .[10] When E_t is combined with E together, the resulting equation is a linear equation in terms of the changes in the vapor temperatures of bubbles K-1, K, and K+1, which looks like:

$$C_1(K) \quad T(K \quad 1) + C_2(K) \quad T(K) + C_3(K) \quad T(K+1) = C_4(K) \quad (15)$$

In general, if a series of N bubbles of uniform vapor pressure extends from the

bottom to top of the channel, then temperature changes in the N bubbles are calculated by solving a set of linear equations written in terms of N unknowns. Once the vapor temperatures are known, the saturation conditions are used to obtain the vapor pressures.

3. Overview of Basic Calculation Scheme

The calculation sequence for the present model is summerized as following steps:

(1) It first reads input variables that users must supply and then determines the steady state conditions for the coolant temperature and pressure distributions, wall temperatures in the channel. It also defines various initial conditions for the transient calculation.
(2) Calculate the preliminary flow rate and coolant temperature distributions together with the advanced wall temperatures, in each liquid slug.
   - Neglecting the effect of changes in the vapor pressures over the time step
(3) Calculate the advanced vapor temperatures if there were vapors in the channel. Iterative process is necessary in this calculation, because calculation of the interface heat transfer requires the advanced vapor temperature.
(4) Compute the advanced mass flow rates and temperatures taking into account the vapor pressure changes.
(5) Check a new vapor formation

During the calculation, the time step is reduced when the flow rate change is radical, the vapor temperature change is large, or number of iteration is so many.

4. Results

The KALIMER design parameters for the active core channel are used in order to verify the SOBOIL model and they are summarized in Table 1. The initial values for

Table 1 Parameters for SOBOIL verification

Parameters	Values used in **SOBOIL**	Parameters	Values used in **SOBOIL**
Active Core Height (m)	1.2	Fuel Pallet Radius (m)	2.73×10^{-3}
Flow Area (m^2)	2.87×10^{-5}	Cladding Inner Radius (m)	3.15×10^{-3}
Hydraulic Diameter (m)	2.87×10^{-5}	Cladding Outer Radius (m)	3.70×10^{5}
Perimeter (m)	0.0074	Time-Step (ms)	5.0
Initial Liquid Flow (kg/s)	0.14686	No. of Axial Nodes	20
Inlet Coolant Temp. (°K)	1150.70	No. of Radial Nodes in the Fuel Pallet	6
Inlet Coolant Pressure (Pa)	4.30×10^{5}	No. of Radial Nodes in the cladding	3
Outlet Coolant Pressure (Pa)	4.0×10^{-5}		

SOBOIL are obtained from the steady state results of SSC-K. Fig. 3 is the steady state axial temperatures profiles in the channel, while Fig. 4 illustrates the radial temperature distributions in the fuel pin with the different axial positions. The fuel temperature at the last junction is seen lower than the down node temperature, since the KALIMER core is designed with lower heat generation in the upper part than in the lower part.

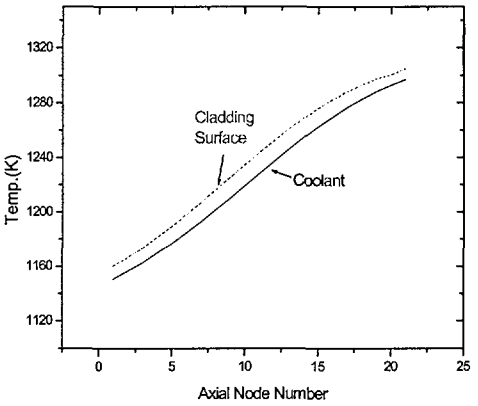

Fig. 3 Steady-State Temp. Profiles

For the transient, the core inlet coolant temperature is assumed to increase 50 °K/sec while the inlet coolant pressure keeps the constant value, taking account of a condition during the ULOHS accident. Since a newly generating vapor gets the saturation pressure corresponding to the specified superheated temperature which is a vapor generation criterion, the vapor pressure is higher than the liquid pressure at that point by the amount of the superheat. Consequently, a pressure jump occurs when a new vapor is generated in the present model. Fig. 5 is calculation of the pressure variation for the first vapor with time. The vapor initially grows due to the pressure jump as well as heat transfer from liquid near the interface into the vapor. The two effects accelerate the vapor growth in the early period but the vapor pressure decreases shortly after the jump. The main reason is the initial volume expansion. As size of the vapor gets larger, amount of heat transfer from the wall (fuel) begins to overwhelm heat transfer from the vapor to

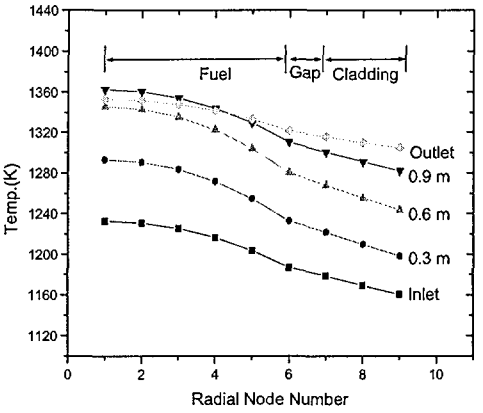

Fig. 4 Temp. Distribution within Fuel Pin

the liquid at the interface. Then, the pressure goes up quickly again. The fast increase of the vapor pressure also causes the lower interface of the vapor to move downward rapidly. The sudden increase of the vapor pressure near 0.75 sec in Fig. 5 gives rise to reduction of the flow rate for the liquid slug below the vapor, since pressure difference for the upper and lower boundaries in the liquid slug gets smaller. The flow behavior is well explained from the result in Fig. 6. Accordingly, the wall heat transfer as well as reduction of the flow rate for the liquid slug below the vapor, mostly contributes to the rapid development of the lower interface of the vapor around 1.0 sec as shown in Fig. 7. The sudden enlargement of the vapor region, on the contrary, leads to slowing down the pressure increase. The flow rate for the liquid slug under the vapor subsequently recovers as the vapor pressure gets lower.(Fig. 6) Finally, amount of the heat transfer from the wall and that from the vapor to the liquid near the interface are almost balanced as the vapor gets larger. The vapor behavior thereafter slows down and the lower interface of the vapor changes smoothly until another vapor is formed below the first vapor at about 3.625 sec. The initial bubble behavior is more clearly confirmed through the result from behavior of the second vapor represented from Fig. 8 to 11. The initial increase of the pressure reduces the liquid flow rate similar to the former vapor and the upper interface moves upward much faster than the lower interface. It

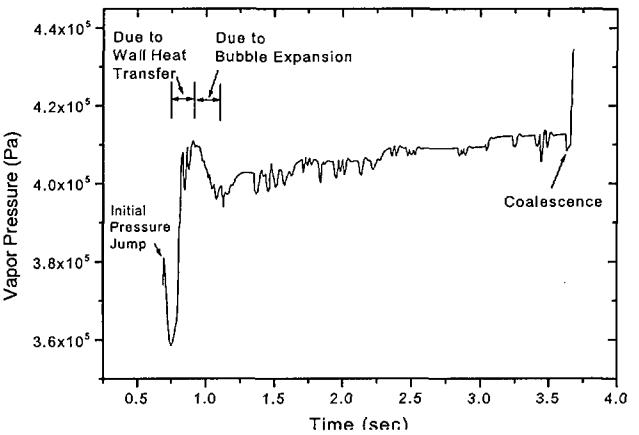

Fig. 5 Vapor Pressure Change

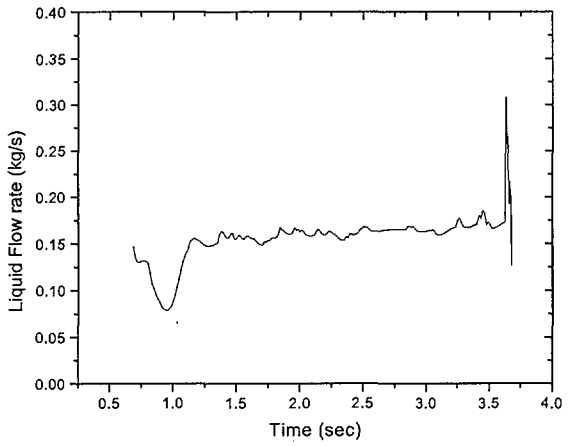

Fig. 6 Liquid Flow in the Liquid Slug

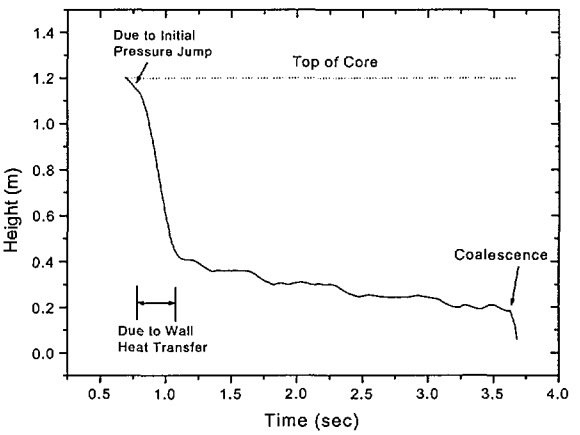

Fig. 7 Change of Lower Interface of Vapor

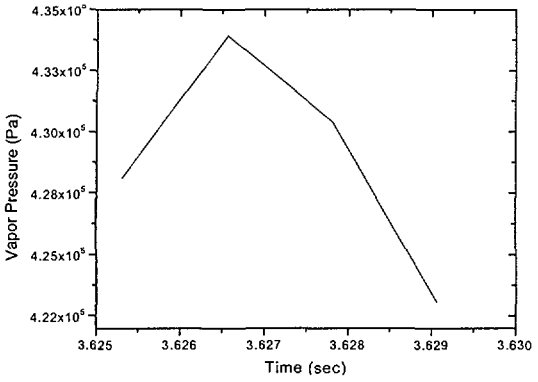

Fig. 9 Liquid Flow in the Liquid Slug

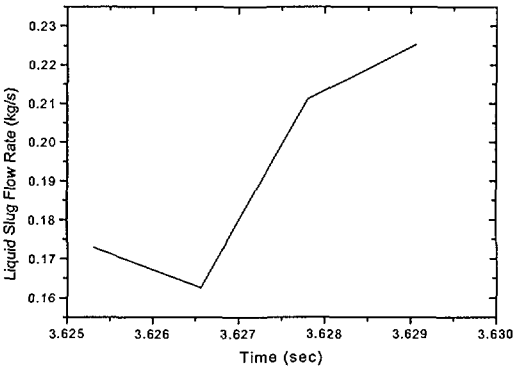

Fig. 8 Vapor Pressure Change

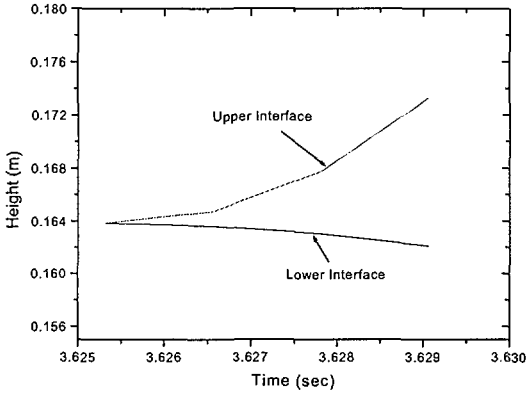

Fig. 10 Change of Lower Interface of Vapor

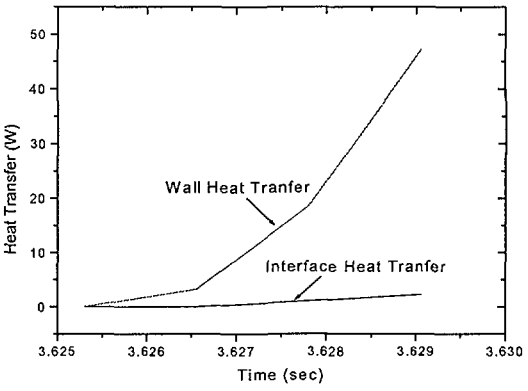

Fig. 11 Heat Transfers into Vapor

is obviously demonstrated from Fig. 11 that the wall heat transfer influences dominantly to the vapor expansion. The liquid slug located above the new vapor gets shorter. On the other hand, the liquid flow rate is smaller compared with that below the vapor. In the SOBOIL model, when the gap distance between two vapors reduces to be smaller than a specified length, two vapors are to coalesce and merge into one. Another drastic development of the lower interface around 3.63 sec in Fig. 7 corresponds to consequence of the coalescence. The second vapor exists only for ~ 4 ms. Since pressure of the merged vapor from the coalescence is an averaged pressure of the two vapor pressures at the present time, it shows a peak shape in Fig. 5. Similarly, the liquid flow rate also shows a peak behavior around this time because it is replaced with the liquid flow rate for the liquid slug below the disappearing vapor.

5. Discussions

The steady state calculation looks to be reasonable. As power generation goes up, the slope of the coolant temperature along the flow direction also increased. it

smoothens out as the slope decreases. Generally the vapor formation and its initial growth also follow the behavior qualitatively assumed in the present model. The initial vapor growth is similar to the results shown in CABRI analysis using FRAX-5 and SAS4A [6,9], where the sudden enlargement of the vapor region downward was predicted within a short time, ~ ms. The homogenous model which assumes saturation condition, uniform pressure and temperature distributions within a vapor is known to be not valid when a vapor size does exceed a certain value. Thus, the vapor temperature as well as pressure may not be likely to be same within such a large vapor. The vapor flow rate cannot be calculated with the similar equation as applied to the liquid slug, since vapor must be treated as a compressible fluid. For small bubbles the pressures are uniform spatially inside the bubbles, whereas there exists pressure gradient for a bubble length exceeding a specified minimum size. Thus, a different model must be applied to a large bubble. This model will be considered later.

Some user specified parameters such as the conditions for vapor formation, a liquid gap distance for the vapor coalescence, time-step reduction criteria, etc. are not physically justified. However, most of physical phenomena seem to be reasonable at least qualitatively so that a basis for complete sodium boiling model must be established. It is confirmed that the vapor is obviously the driving force for motion of the liquid slug. The vapor pressure is quite sensitive not only to volume change of vapor, but also to the liquid slug flow, as shown in the results. The balance between the wall and interface heat transfers also affects the vapor volume change directly. It is noted that if the general model is applied to the present problem, flow reversal might be possible. An additional model which can describe large vapor behavior, should be necessary for complete analysis of the sodium boiling along with more sophisticated verification for its validity.

As shown in the results, the sodium voiding develops so rapidly that the reactivity insertion in the KALIMER core may be large within a short period enough to threaten the fuel pin integrity during the accidents under which sodium boiling is anticipated. Therefore, it is very important to predict the phenomena accurately for understanding the fuel behavior due to the reactivity feedback. The effort will be made to improve the limitations continuously and, finally, it will be coupled to SSC-K to extend the code capability.

Acknowledgement

This work was performed under the Long-term Nuclear R & D Programs sponsored by the Korea Ministry of Science and Technology.

Nomenclatures

G = liquid mass flow rate (kg/s-m^2)
r_ℓ = liquid density
c_ℓ = liquid specific heat
j (z,t) = wall heat flow per unit coolant volume (w/m^3)
$Q_c(z,t)$ = volume source due to direct heating by neutrons and gamma rays (w/m^3)

r = r (z)

$c = c(z)$

$d_1 = \dfrac{t}{2 r c}$

$h_1 = h_{eci}(t)$

$h_2 = h_{eci}(t + t)$

$j_1 = h_{ec}(z,t + t)T_e(z,t + t) + h_{ec}(z,t)T_e(z \quad z,t)$

x = u or ℓ
A_{cx} = Area of coolant channel
$T_{\ell x}$ = Liquid temperature near interface
k_ℓ = Liquid thermal conductivity near interface
a = $k_\ell / r_\ell C_\ell$, the thermal diffusivity of liquid sodium
Q = heat input per unit volume in the liquid
= distance into liquid slug from liquid-vapor interface
x = z - z_i for upper interface
x = - (z – z_i) for lower interface
t' = time since the vapor bubble started to form

References

[1] Dohee, Hahn, et al., "KALIMER Preliminary Conceptual Design Report",

KAERI/TR-1636/2000

[2] G.A. Greene, T. Ginsberg, and M.S. Kazimi, "Assessment of the Thermal Hydraulic Technology of the Transition Phase of a Core-Disruptive Accident in a LMFBR", NUREG/CR-3014, Nov. 1982

[3] Alan E. Waltar and Albert B. Reynolds, Fast Breeder Reactors II', Pergamon Press, New York, Oxford, Toronto, Sydney, Paris, Frankfurt

[4] F.E. Dunn, et al., "The SAS2A LMFBR Accident-Analysis Computer Code," ANL-8183, Oct. 1974

[5] Y.M. Kwon, et al., "SSC-K Code User' s Manual (Rev. 0)", KAERI/TR-1619/2000

[6] Y.S. Tang, et al., "Thermal Analysis of Liquid-Metal Fast Breeder Reactors", ANS, 1978

[7] M. Green, "FRAX, A Whole Core Accident Code for Fast Reactors", AEA Presentations to KAERI, March 1998

[8] D.J. Brear, J.A. Moran, T. Rudge, "Fuel Pin loading and pin failure criteria in the UK code FRAX-5 under WCA condition", Fast Reactor Core and Fuel Structure Behavior, BNES, London, 1990

[9] T. Rudge, "Homsep-2 : A One-dimensional Sodium Boiling Model for the Fast Reactor", Nucl. Energy, 1989, 28, N0. 3, June, 171-181

[10] W.P. Chang, et al., "Development of Two-phase Flow, 'SOBOIL', for Sodium", . KAERI/TR-1636/2000